J. Fluid Mech. (2004), *vol.* 521, *pp.* 251–271. © 2004 Cambridge University Press
DOI: 10.1017/S0022112004001855 Printed in the United Kingdom

Critical assessment of turbulent drag reduction through spanwise wall oscillations

By MAURIZIO QUADRIO AND PIERRE RICCO†
Dipartimento di Ingegneria Aerospaziale del Politecnico di Milano, via La Masa 34, 20158 Milano, Italy

(Received 15 August 2003 and in revised form 16 July 2004)

Direct numerical simulations of the incompressible Navier–Stokes equations are employed to study the turbulent wall-shear stress in a turbulent channel flow forced by lateral sinusoidal oscillations of the walls. The objective is to produce a documented database of numerically computed friction reductions. To this aim, the particular numerical requirements for such simulations, owing for example to the time-varying direction of the skin-friction vector, are considered and appropriately accounted for.

A detailed analysis of the dependence of drag reduction on the oscillatory parameters allows us to address conflicting results hitherto reported in the literature. At the Reynolds number of the present simulations, we compute a maximum drag reduction of 44.7%, and we assess the possibility for the power saved to be higher than the power spent for the movement of the walls (when mechanical losses are neglected). A maximum net energy saving of 7.3% is computed.

Furthermore, the scaling of the amount of drag reduction is addressed. A parameter, which depends on both the maximum wall velocity and the period of the oscillation, is found to be linearly related to drag reduction, as long as the half-period of the oscillation is shorter than a typical lifetime of the turbulent near-wall structures. For longer periods of oscillation, the scaling parameter predicts that drag reduction will decrease to zero more slowly than the numerical data. The same parameter also describes well the optimum period of oscillation for fixed maximum wall displacement, which is smaller than the optimum period for fixed maximum wall velocity, and depends on the maximum displacement itself.

1. Introduction

A number of recent papers have shown that wall-bounded turbulent flows, both in the planar and cylindrical geometry, exhibit interesting modifications when cyclic surface motions are imposed in the spanwise direction, or when an oscillating spanwise pressure gradient is applied. This emerges from numerical studies based on the direct numerical simulation (DNS) of the incompressible Navier–Stokes equations, as well as from laboratory experiments. In the group of numerical papers, we mention the first work on the subject by Jung, Mangiavacchi & Akhavan (1992), and the extension of the results from the plane channel flow to the pipe flow by Quadrio & Sibilla (2000). Among the experimental studies, we recall the first investigation by Laadhari, Skandaji & Morel (1994) and the study by Choi (2002). Karniadakis & Choi (2003) discussed the properties of the oscillating wall in connection with related flow modifications, such as for example the use of a spatially or temporally oscillating spanwise-oriented Lorentz force in the near-wall region of a turbulent flow of an electrically conducting fluid, described by Berger *et al.* (2000), and the excitation of the flow with transverse travelling waves presented by Du, Symeonidis & Karniadakis (2002).

---

† Present address: Department of Mathematics, Imperial College, 180 Queen's Gate, London SW7 2BZ, UK.

Perhaps the most interesting and practically appealing among the effects of the oscillating wall on turbulent flows is the significant reduction of the mean streamwise wall friction, first reported by Jung *et al.* (1992). Despite the studies available in the literature, there are a number of issues related to the drag-reduction properties of the oscillating wall that have not yet received a definite answer. These issues, which are important both from a fundamental and an applicative point of view, are reviewed briefly in §§ 1.1, 1.2 and 1.3. We also mention an additional problem, which is relevant to an eventual practical application of the oscillating wall as a drag-reducing technique: the dependence of the drag reduction on the Reynolds number of the flow. This topic is not addressed in the present work.

1.1. *Maximum drag reduction*

The available data in boundary layers and channel flows, collected at relatively low values of the Reynolds number, indicate that the oscillation of the wall causes a significant decrease of the mean level of the turbulent skin-friction compared with the value over a fixed wall, even though it is not capable of relaminarizing the turbulent flow. However, it appears that the exact value of such an important quantity as the maximum drag reduction has not yet been assessed. Jung *et al.* (1992), Baron & Quadrio (1996), Choi, DeBisschop & Clayton (1998), Nikitin (2000), Quadrio & Sibilla (2000), J.-I. Choi, Xu & Sung (2002) and Choi (2002) have reported that reductions of 40% or more can be reached by proper choices of the parameters of the wall oscillation. On the other hand, Skandaji (1997) (whose work was also published in Laadhari *et al.* 1994), Trujillo, Bogard & Ball (1997) and Choi & Graham (1998) have indicated lower maximum drag-reduction values, namely 35%, 27% and 25%, respectively. It is puzzling to observe that numerical investigations agree on indicating larger drag reductions than those predicted by laboratory experiments.

1.2. *Net energy saving*

A second open issue concerns the global energetic balance of the oscillating wall as a drag-reduction technique. Since external power is required to move the wall against the viscous resistance of the fluid, it is important to determine the parameters of the oscillation yielding the best overall performance, considering both energetic costs and benefits, and to verify whether this technique can lead to a net gain, at least in an idealized situation when the mechanical losses of a real oscillating device are neglected. A similar energy budget was evaluated by Berger *et al.* (2000) for the aforementioned Lorentz force technique. They showed that the power required to generate the magnetic force is approximately one order of magnitude larger than the power saved owing to the reduced friction drag, when closed-loop control schemes are considered. Furthermore, for open-loop control schemes, which are more directly related to the movement of the wall considered in the present work, they found that the balance is extremely unfavourable. Indeed, the ratio between the power required to generate the force and the power saved was $O(1000)$ for that case. On the contrary, studies on the oscillating-wall technique present more promising results. Baron & Quadrio (1996) for a plane channel flow and Quadrio & Sibilla (2000) for a pipe oscillating about its axis have indicated that the power saved and the power required for the movement of the wall may be of the same order of magnitude, thus suggesting the possibility of a positive net energy balance for certain values of the oscillation parameters. These results, however, were obtained from preliminary computational studies, certainly affected by the limited spatial and temporal discretization. No definite conclusion concerning the very existence and extent of a region of positive energy balance in the parameter space can thus be drawn to date, although these results indicate a possible global energy benefit.

1.3. *Scaling of drag reduction*

General agreement is also lacking on the scaling of drag reduction, namely on the existence of a quantity that is a function of the oscillation parameters, to which the amount of drag reduction uniquely relates. Trujillo *et al.* (1997), Choi *et al.* (1998), Choi & Graham (1998), Choi (2002) and Karniadakis & Choi (2003) have suggested that drag reduction depends neither on the maximum peak-to-peak spatial displacement D_m of the wall, nor on the oscillation period T, taken as independent parameters, but it scales with the maximum wall velocity $W_m = \pi D_m / T$. On the other hand, Jung *et al.* (1992), Baron & Quadrio (1996), Dhanak & Si (1999), Quadrio & Sibilla (2000) and Nikitin (2000) have not been able to find a scaling parameter, but determined the existence of an optimal period of 100–125 viscous time units for fixed maximum wall velocity. This optimal period has been related to the thickness of the transversal laminar Stokes layer which maximizes the interaction of the moving wall with the near-wall turbulent structures.

J.-I. Choi *et al.* (2002) have addressed the issue of the scaling of drag reduction, proposing two parameters related to the decrease of the skin-friction coefficient. The first one is a critical wall-normal distance to which spanwise friction effects diffuse. This length is defined by means of the Stokes solution for an oscillating laminar boundary layer, and represents the position where the maximum velocity during the cycle is higher than a given threshold. Turbulent structures within this distance from the wall are influenced by the wall oscillation, whereas the effects of the motion are not felt farther from the wall. The second parameter is the acceleration of the Stokes layer. Its importance follows from the observation that in a steadily rotating pipe, where there is no spanwise acceleration, the skin-friction attenuations are smaller, as pointed out by Quadrio & Sibilla (2000), who compared their results for an oscillating pipe with those by Orlandi & Fatica (1997) for a steadily rotating pipe. The amount of drag reduction shows some correlation with each of these two parameters, and the correlation increases when the two quantities are combined in a unique factor. However, some available experimental data not considered by J.-I. Choi *et al.* (2002) (for example the data of Jung *et al.* (1992) at $T^+ = 200$ and $T^+ = 500$) appear to be poorly correlated with the proposed scaling quantity.

1.4. *Objective and layout*

In this work, we use an incompressible Navier–Stokes equations solver to perform direct numerical simulations of a turbulent channel flow over spanwise-oscillating walls. The main objective is to produce a well-documented and reliable database, which provides a complete map of drag-reduction data versus the parameters defining the oscillation of the wall, namely the maximum wall velocity W_m, the oscillation period T and the maximum wall displacement D_m. Our measurements of streamwise friction from DNS are reported, and emphasis is placed on computational procedures and error analysis, in order to estimate the measurement error. We then address the three open questions illustrated above, also capitalizing on the recent analysis of the initial transient of the flow after the start-up of the oscillation, developed by Quadrio & Ricco (2003).

The layout of the paper is as follows. All the numerical issues are discussed in the following section: the numerical method and the computing system are briefly illustrated in § 2.1; the adopted spatial and temporal discretization is described in § 2.2; the computational procedures to calculate the mean value of the friction coefficient are detailed in § 2.3; validation issues and error estimates are discussed in § 2.4. Drag-reduction data are presented in § 3, first in terms of maximum absolute savings in § 3.1 and then considering the net power savings in § 3.2. The discussion of these topics in view of the other data available in the literature, and the issue of their scaling, are contained in § 4. Lastly, § 5 is devoted to conclusions.

2. Problem definition and numerical issues

2.1. *Numerical method and computing system*

The computer code used in the present work has been developed by Quadrio & Luchini (2001), and solves the incompressible Navier–Stokes equations for the turbulent flow in a plane channel. The equations are written in terms of two scalar equations for the wall-normal component of the velocity and vorticity vectors, following a procedure which eliminates the pressure, described for example in Kim, Moin & Moser (1987). The code is based on Fourier expansions in the homogeneous directions, and fourth-order-accurate compact finite-differences schemes are used in the wall-normal direction. Compact schemes offer a discrete differentiation with resolution comparable with that of spectral schemes (Lele 1992), and at the same time allowed us to design a numerical method with significant advantages from the point of view of parallel computing.

The nonlinear terms of the equations are evaluated in a pseudo-spectral way, and the related aliasing error (in the homogeneous directions) is exactly removed by expanding the number of Fourier modes by a factor of at least $3/2$ before transferring from Fourier space into physical space. Time integration of the equations is performed with the classical partially implicit approach, using a third-order low-storage Runge–Kutta method for the convective terms, and a second-order Crank–Nicolson scheme for the viscous terms.

Our code is able to exploit the computing power of shared-memory SMP machines, and connects together multiple machines for distributed parallel computing. An innovative parallel strategy is adopted so that the communication is reduced to a minimum: during the computations a global transpose of the data is never required, thus allowing for the use of commodity networking hardware. The overall amount of required memory can be subdivided among the computing nodes. When run with a time-integration scheme that requires one preceding time level (such as the third-order Runge–Kutta used in the present work), the code requires a storage space of the order of $5N_xN_yN_z$ floating-point variables, N_x and N_z being the number of Fourier modes in the homogeneous directions, and N_y the number of points in the wall-normal direction.

The numerical simulations described in this paper have been performed on a dedicated purpose-built computing system, made by 8 commodity SMP Personal Computers, each equipped with two Intel Pentium III CPU at 733 MHz, with 256 MB RAM and two cheap Fast Ethernet cards. The computing nodes are connected together in a dedicated ring-like connection topology which avoids any hubs or switches, and replicates the way data are stored in the machines during the computations.

As demonstrated by Kim *et al.* (1987), the periodic boundary conditions implied by the Fourier expansions can be adopted in the homogeneous directions, provided the computational domain is large enough. At the channel walls, the usual no-slip and no-penetration conditions are applied. The wall boundary condition for the spanwise (z) component of velocity is:

$$W = W_m \sin\left(\frac{2\pi}{T}t\right),$$

i.e. the two walls move in phase with a spanwise velocity W which is a sinusoidal function of time t with prescribed period T and amplitude W_m. For ease of comparison with previous studies, the calculations are performed at a reference value of the Reynolds number of $Re_\tau = 200$, being Re_τ based on u_τ, the friction velocity in the uncontrolled case, and on h, half the distance between the channel walls.

2.2. *Discretization*

The streamwise (x) length of the computational domain is $L_x = 21h$, and the spanwise (z) width is $L_z = 4.2h$. The x-direction is discretized with 321 Fourier modes; 129 modes are used in the spanwise (z) direction, and the number of collocation points in the wall-normal (y) direction is 129. The spatial resolution in the reference case is $\Delta x^+ = 13.1$, $\Delta z^+ = 6.5$ and $\Delta y^+ = 0.8 - 5.4$ (the $+$ superscript indicates quantities made dimensionless with inner variables, i.e. with the friction velocity of the reference case and the kinematic viscosity ν of the fluid). The dimensions of the periodic box and the spatial resolution are comparable with those currently used in the literature for similar values of the Reynolds number (see for example, Kim *et al.* 1987; Moser, Kim & Mansour 1999). The streamwise extent of the computational box is, however, significantly larger, since it is known (Orlandi & Fatica 1997) that the near-wall turbulent structures are more elongated under drag-reducing conditions. The effective resolution in wall units becomes much higher for the cases with drag reduction, owing to the significant decrease in u_τ.

The total integration time is $t_{tot} = 1000\, h/U_P$, where U_P is the centreline velocity of a laminar Poiseuille flow with the same flow rate. This time interval corresponds in viscous units to $t^+_{tot} \approx 8400$, and to $\approx 1250\, h/U_c$ where U_c is the mean velocity at the centreline of the channel. This is significantly longer than the time interval usually considered for the reliable calculation of low-order turbulence statistics in standard DNS at similar Reynolds numbers. This value of t_{tot} corresponds to more than 30 wash-out times of the present very long computational domain (the wash-out time is defined by del Álamo & Jiménez (2003) as $t\, U_b/L_x$, where U_b is the bulk velocity). The statistical sample is further increased by a factor of two by ensemble-averaging over both walls. The reference case without wall oscillation and the cases with the largest absolute and net drag reduction (cases 0, 20 and 25 in table 2) are integrated for a longer time interval, namely $1500\, h/U_P$. The time step used in the computation is smaller than that imposed by the stability limit of the time-integration scheme, in order to minimize errors from the temporal discretization. It is set to $\Delta t^+ \approx 0.16$ for the reference case, and reduces to $\Delta t^+ \approx 0.1$ for the cases with large drag reduction. To improve time accuracy, the calculations are performed in a reference frame which moves in the streamwise direction at a velocity slightly lower than the bulk mean velocity of the flow.

2.3. *Computational procedures*

The equations of motion are integrated in time, always starting from the same unperturbed flow field as the initial condition, with the main purpose of calculating an average value of the wall friction. The longitudinal flow rate is kept constant during the simulations, allowing the space-averaged longitudinal friction to fluctuate in time around its time-mean value. A null instantaneous spanwise pressure gradient is imposed.

The time history of the two components of the wall-averaged friction is recorded from the simulations. In the post-processing phase, the time histories over the two walls are combined, and the time average over the maximum available number of integer multiples of the wall oscillation period is computed after discarding the initial transient. The oscillating movement of the walls starts at $t = 0$; the initial conditions correspond to an unmanipulated flow, which is in statistical equilibrium for the fixed-wall condition. A certain amount of time is consequently needed for the flow to adapt to the new boundary conditions and to reach its new quasi-equilibrium state. The initial transient phase is carefully discarded. This operation is crucial for a reliable measurement of drag reduction in numerical simulations, where the total integration time is limited by cost considerations. The early-stage flow regime after the start-up of the oscillatory motion, and in particular the length of the initial transient, have been the object of the analysis by Quadrio & Ricco (2003). They determined that this transient can be non-monotonic, that it presents different durations for different flow variables, and that the duration strongly depends on the maximum wall velocity W_m. In the present study, we are not interested in the precise determination of the duration of the initial transient for the longitudinal friction. Based on a visual case-by-case observation of the time history, the instant t_i where the statistical analysis can be started is simply identified when an interval significantly longer than the initial transient has elapsed. While not optimally efficient, this procedure allows us to safely remove the effects of the initial transient from the time average. For each computational case, the chosen value of t_i is reported in table 2.

2.4. *Error estimation*

The fundamental quantity measured in our numerical simulations is the friction drag, quantified by the friction coefficient:

$$C_f = \frac{2\tau_x}{\rho U_b^2},$$

where ρ is the density of the fluid, τ_x is the longitudinal component of the shear stress at the wall, and U_b is the bulk velocity.

The computed value of C_f in the reference simulation at $Re_\tau = 200$ is 7.93×10^{-3}. It compares very well (within a 0.4% difference) with the value reported by Kim *et al.* (1987), after rescaling to account for their different Reynolds number ($Re_\tau \approx 180$), and by assuming $C_f \sim Re_\tau^{-0.25}$. This is a commonly accepted dependence of C_f on Re, first proposed by Dean (1978). The comparison of our measured C_f with results from Dean's correlation is not totally satisfying, with a 3% disagreement, but an identical disagreement is also present in Kim *et al.*'s results, and it may well be due to the non-optimal value predicted by the empirical correlation at low values of the Reynolds number.

We have tested the sensitivity of the measured value of the friction coefficient to various discretization parameters. The adopted size of the time step does not cause any appreciable error in the time-average measure of C_f, as verified in a number of preceding works and, in particular, for the present numerical scheme, by Quadrio & Luchini (2003). Additional discretization checks are described in table 1. We first performed a fixed-wall simulation with less spatial resolution, in a smaller

	L_x/h	L_z/h	N_y	N_x	N_z	Δy^+_{max}	Δx^+	Δz^+	$t_{tot}U_P/h$	$10^3 C_f$	Error (%)
Case 0	21	4.2	129	321	129	5.4	13.1	6.5	1000	7.93	–
Check a_1	*4π*	4.2	129	*161*	129	5.4	*15.7*	6.5	*500*	7.88	–0.6
Case 25	21	4.2	129	321	129	3.0	7.3	3.6	1000	4.40	–
Check a_2	21	4.2	129	*513*	129	3.0	*4.5*	3.6	1000	4.37	–0.4
Check b_2	21	4.2	*257*	321	129	*1.5*	7.3	3.6	1000	4.33	–0.8
Check c_2	21	*2π*	129	321	*257*	3.0	7.3	*2.7*	1000	4.37	–0.3

TABLE 1. Percentage error in the calculation of C_f as a function of the discretization parameters. Checks are performed for cases 0 (no wall oscillation) and 25 (nearly maximum drag reduction) described in table 2. The parameters which are different from the base discretization described in § 2.2 are printed in italics. Data in inner units for case 25 are computed with the actual friction velocity.

computational domain and for a shorter time interval. This less-resolved simulation, indicated as check a_1 in table 1, is still one of notable computational size, and it has given a friction coefficient only –0.6% different from that of the reference simulation.

Since it is not immediately evident how the movement of the walls affects the resolution requirements, one case which yields nearly the maximum drag reduction (case 25 in table 2) has been the subject of three additional resolution checks, described as checks a_2, b_2 and c_2 in table 1. When the wall oscillates, it is known that the near-wall low-speed streaks cyclically incline to an angle, as visualized by Quadrio & Ricco (2003). The large local spanwise gradients are then partly converted to streamwise gradients, thus increasing the resolution requirements in the streamwise direction. Check a_2, in which the streamwise resolution is almost doubled, has yielded a friction coefficient of $C_f = 4.37 \times 10^{-3}$, with only a –0.4% difference in the drag reduction. Indeed, the increase in resolution requirements is balanced by the decrease in the friction Reynolds number caused by the oscillation of the wall. In check b_2, the number of points in the wall-normal direction has been doubled, obtaining a difference of –0.8%. Lastly, in check c_2, the spanwise resolution has been increased and at the same time a wider computational domain has been considered: in this case the difference is only –0.3%.

3. Drag reduction results

We have explored the drag reduction characteristics of the oscillating wall by computing the time-averaged value of the friction coefficient in a reference simulation at $Re_\tau = 200$ and in 37 additional computational cases, in which the period T of the sinusoidal oscillation and its maximum velocity W_m have been varied independently. The oscillation of the wall is described by a third parameter, namely its maximum displacement D_m. However, only two of them are independent, since for a sinusoidal oscillation $D_m = W_m T/\pi$. The whole set of simulations is documented in table 2 in terms of the parameters of the oscillation, the measured friction coefficient and the power budget. The time t_i indicates the initial time at which the averaging procedure is started after the initial transient, cf. § 2.3. The scaling parameter S^+ is discussed in § 4.3.

3.1. *Absolute drag reduction*

The percentage of friction power P_{sav} saved thanks to the oscillation of the walls is reported in table 2. P_{sav} is defined as follows:

$$P_{sav} = \frac{U_b L_x L_z}{t_f - t_i} \int_{t_i}^{t_f} \left[\left(\tau_{x,0}^{(\ell)} - \tau_x^{(\ell)} \right) + \left(\tau_{x,0}^{(u)} - \tau_x^{(u)} \right) \right] \mathrm{d}t,$$

Case	T^+	W_m^+	D_m^+	$t_i U_P / h$	$10^3 C_f$	$\% P_{sav}$	$\% P_{req}$	$\% P_{net}$	S^+
0	∞	0	0	0	7.93	−0	0	0	0.0000
1	5	4.5	7	50	7.90	0.3	−54.0	−53.7	0.0142
2	10	2.5	8	100	7.89	0.5	−11.4	−10.9	0.0241
3	15	18	86	100	6.69	15.6	−481.3	−465.7	0.1387
4	30	4.5	43	100	7.33	7.5	−20.8	−13.3	0.1114
5	30	12	115	150	6.21	21.7	−147.9	−126.2	0.1940
6	30	18	172	100	5.77	27.2	−332.8	−305.6	0.2282
7	30	27	258	150	5.39	32.1	−748.6	−716.5	0.2624
8	50	18	286	100	5.21	34.3	−256.6	−222.3	0.2799
9	67	11.3	241	150	5.46	31.2	−87.8	−56.6	0.2482
10	75	4.5	107	100	6.66	16.0	−13.0	3.0	0.1490
11	75	12	286	150	5.36	32.4	−92.9	−60.5	0.2596
12	75	18	430	200	4.89	38.3	−209.1	−170.8	0.3053
13	75	27	645	200	4.58	42.3	−470.3	−428.0	0.3510
14	100	4.5	143	150	6.55	17.4	−11.2	6.2	0.1534
15	100	12	382	150	5.33	32.8	−80.1	−47.3	0.2672
16	100	18	573	200	4.82	39.1	−180.7	−141.6	0.3143
17	100	27	859	250	4.39	44.7	−407.1	−362.4	0.3613
18	125	1.5	60	150	7.62	3.8	−1.0	2.8	0.0261
19	125	3	119	100	7.08	10.7	−4.3	6.4	0.1070
20	125	4.5	179	100	6.57	17.2	−9.9	7.3	0.1544
21	125	6	239	150	6.17	22.1	−17.7	4.4	0.1880
22	125	9	358	150	5.72	27.9	−40.0	−12.1	0.2353
23	125	12	477	200	5.35	32.5	−71.4	−38.9	0.2689
24	125	18	716	200	4.81	39.3	−161.2	−121.9	0.3163
25	125	27	1074	300	4.40	44.5	−363.1	−318.6	0.3636
26	150	4.5	215	150	6.65	16.1	−9.0	7.1	0.1537
27	150	18	859	200	4.91	38.1	−146.8	−108.7	0.3150
28	200	4.5	286	150	6.92	12.7	−7.7	5.0	0.1504
29	200	12	764	200	5.77	27.2	−55.8	−28.6	0.2621
30	200	18	1146	200	5.32	32.9	−126.4	−93.5	0.3082
31	200	27	1719	200	5.11	35.5	−285.5	−250.0	0.3543
32	250	4.5	358	100	7.14	10.0	−7.0	3.0	0.1462
33	300	4.5	430	100	7.29	8.1	−6.4	1.7	0.1420
34	300	18	1719	100	6.62	16.5	−104.7	−88.2	0.2909
35	500	12	1910	100	7.52	5.1	−38.7	−33.6	0.2215
36	500	18	2865	100	7.82	1.4	−89.8	−88.4	0.2606
37	750	12	2865	100	7.91	0.2	−35.7	−35.5	0.1982

TABLE 2. Power budget data for different oscillatory conditions, namely period T^+, maximum wall velocity W_m^+ and maximum wall displacement D_m^+ (case 0 refers to the stationary wall configuration). t_i indicates the start of the time-averaging procedure for the calculation of the friction coefficient C_f. P_{sav} is the power saved to drive the flow thanks to the wall oscillation, P_{req} is the power required to move the walls against the viscous resistance of the fluid, and the net gain P_{net} is given by the algebraic sum of the two. S^+ is the scaling parameter discussed in § 4.3.

where t_i and t_f mark the beginning and the end of the time-averaging procedure, the ℓ and u superscripts refer to the lower and upper wall, respectively, the 0 subscript indicates the fixed-wall case and τ_x indicates the space-averaged value. In table 2, P_{sav} is expressed as a percentage of the friction power in the fixed-wall case, given by:

$$\% P_{sav} = 100 \frac{C_{f,0} - C_f}{C_{f,0}}. \tag{3.1}$$

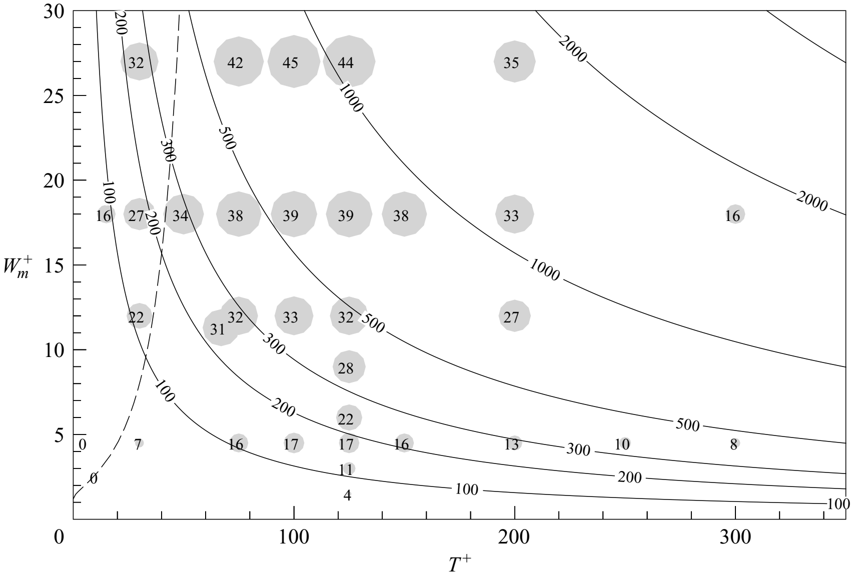

FIGURE 1. Three-dimensional plot of $\% P_{sav}$ versus T^+ and W_m^+. The size of the circles is proportional to the percentage drag reduction, the numerical value of which is reported inside. Hyperbolae are curves of constant maximum displacement D_m^+. The dashed line is the curve of optimum period at fixed displacement, discussed in § 4.3. Note that a few measurement points at high values of T^+ are not shown in the plot.

Figure 1 is a graphical representation of (most of) the drag-reduction data given in table 2, and illustrates the dependency of the percentage drag reduction on the parameters of the oscillation. In the plane of the two considered parameters, i.e. W_m^+ and T^+, the amount of drag reduction is shown with a circle, its area being proportional to the numerical value of the percentage reduction, shown inside the symbol. Lines with constant maximum displacement of the wall are hyperbolae in this plane. The plot reveals that, for a given value of W_m^+, the highest drag reductions can be attained by keeping T^+ in the 100–125 range, and that drag reduction appears to increase monotonically with W_m, for a fixed period of oscillation. Nonetheless, the increase rate of drag reduction with W_m keeps decreasing. For example, at $T^+ = 125$, the power saved changes from 39% to 44%, with the maximum wall velocity increasing from $W_m^+ = 18$ to $W_m^+ = 27$, the highest value of W_m tested in this work.

In figure 2, drag-reduction data are reported as a function of T^+ for three selected values of W_m^+, namely $W_m^+ = 4.5$, 12 and 18. These are three sections of the three-dimensional space shown in figure 1, cut parallel to its horizontal axis. For clarity, measurements are reported using a logarithmic scale for the T^+ axis. For the case dictated by $W_m^+ = 18$, an optimum period of oscillation $T^+ = 125$ guarantees a drag reduction of 39.3%. Periods in the 75–150 range yield amounts of about 40%. Drag reduction appears to increase logarithmically (linearly in log scale) for small T and to reach a maximum at a period weakly (if ever) dependent on W_m. For lower values of W_m, the trend is similar, but smaller drag reductions are achieved. As discussed in § 3.2, optimum values of T^+ and small values of W_m^+ identify an interesting region of the parameter space, where net energy savings are attainable. Also shown in figure 2 is a subset of the available numerical and experimental data, collected at comparable values of W_m^+. A considerable scatter can be seen, with most of the experimental data yielding lower amounts of drag-reduction compared to the present measurements.

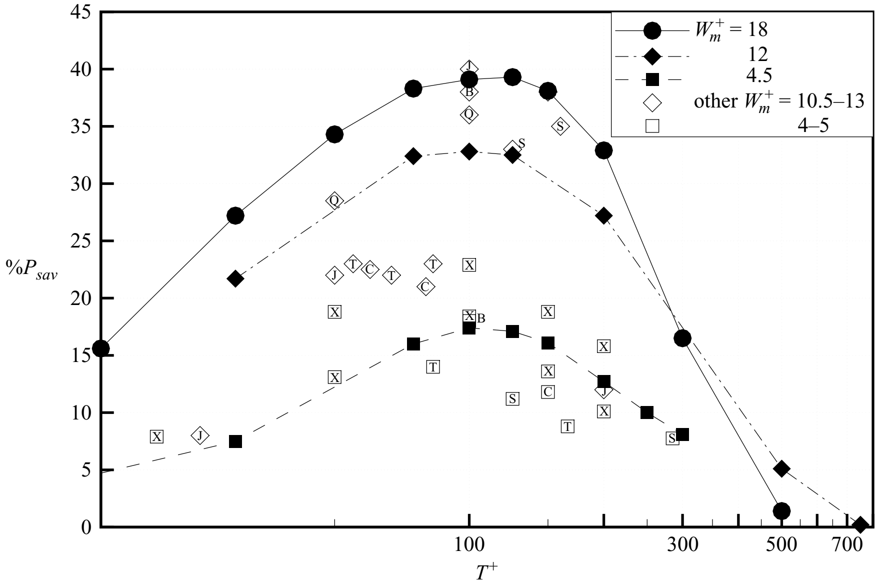

FIGURE 2. $\%P_{sav}$ as a function of period of oscillation T^+, for different values of W_m^+. Open symbols represent comparable data from other measurements, either for $W_m^+ \approx 12$ (diamonds) or $W_m^+ \approx 4.5$ (squares). Letters inside the open symbols are: B, Baron & Quadrio (1996); C, Choi & Graham (1998); X, J.-I. Choi *et al.* (2002); J, Jung *et al.* (1992); Q, Quadrio & Sibilla (2000); S, Skandaji (1997); T, Trujillo *et al.* (1997).

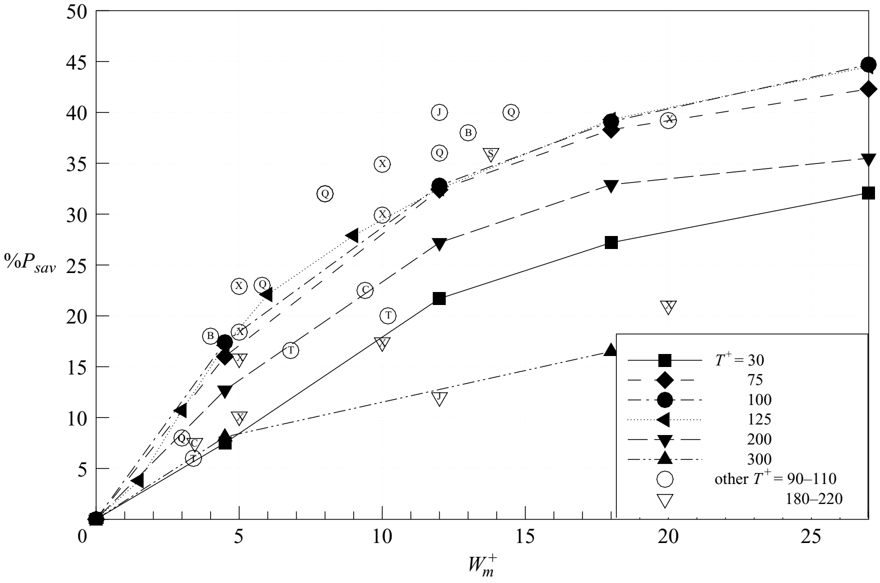

FIGURE 3. $\%P_{sav}$ as a function of maximum wall velocity W_m^+, for different values of T^+. Open symbols represent comparable data from other measurements, either for $T^+ \approx 100$ (circles) or $T^+ \approx 200$ (triangles). For the letters inside the symbols, refer to figure 2.

Figure 3 shows the percentage drag reductions as function of W_m^+ for different values of T^+. The drag reduction monotonically increases with W_m^+ for a given T^+, with an apparent asymptotic behaviour towards a level which seems to depend

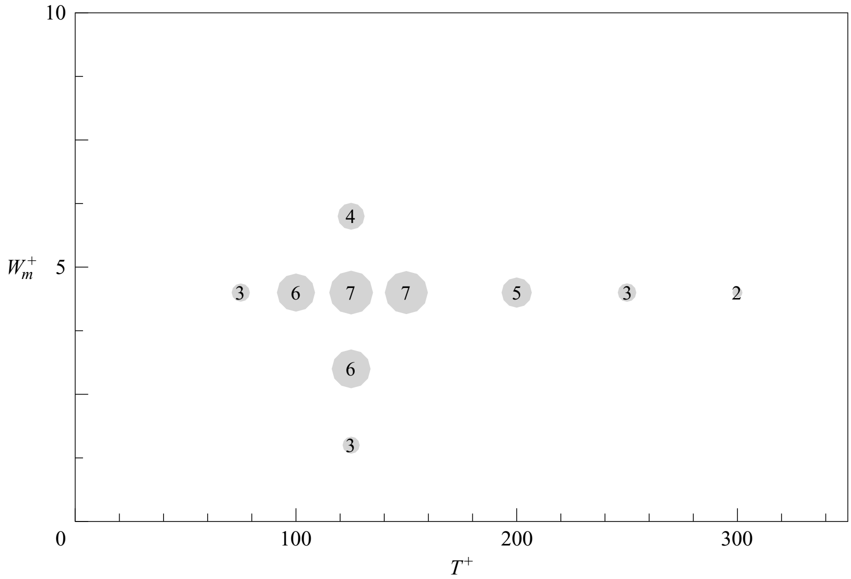

FIGURE 4. Three-dimensional plot of $\%P_{net}$ versus T^+ and W_m^+. The size of the circles is proportional to the percentage net energy balance, the numerical value of which is reported inside. Only points with positive balance are reported.

on T^+. When the period of oscillation is near the optimum value ($T^+ \approx 125$), the amount of drag reduction asymptotically adjusts to approximately 50%. The highest computed value of drag reduction is 44.7%, for $W_m^+ = 27$ and $T^+ = 100$. Again, open symbols in figure 3 show available data, collected mainly at $T^+ \approx 100$, where the previously mentioned trend of numerical simulations yielding larger drag-reduction values compared to experiments is confirmed.

3.2. *Net energy saving*

For a complete assessment of the oscillating wall as a drag-reduction technique, the energetic savings must be compared with the energetic cost of moving the walls. The actual device for wall oscillation can be complex, and it is not our aim to describe it. In the global power budget, we then disregard mechanical losses, which are unavoidable in a real-world implementation. In our computational experiments, we have computed the power P_{req} required for the movement of the walls, defined as:

$$P_{req} = \frac{L_x L_z}{t_f - t_i} \int_{t_i}^{t_f} \left(\tau_z^{(\ell)} + \tau_z^{(u)}\right) W \, \mathrm{d}t, \qquad (3.2)$$

where $W = W(t)$ is the velocity of the two walls and τ_z represents the spanwise wall-averaged component of the wall-shear stress. The required power is given in table 2 as a percentage of the friction power spent in the uncontrolled case. The (algebraic) sum of the percentage powers $\%P_{sav}$ and $\%P_{req}$ is the net energetic balance $\%P_{net}$. This quantity is expressed as savings or losses in the percentage of the friction power in the uncontrolled case:

$$\%P_{net} = \%P_{sav} + \%P_{req}.$$

Figure 4 shows the net percentage saving versus the parameters W_m^+ and T^+ of the oscillation. Only a limited region of the (T^+, W_m^+)-plane is shown, where the budget is positive: this occurs for low values of W_m. The region at high W_m gives larger values

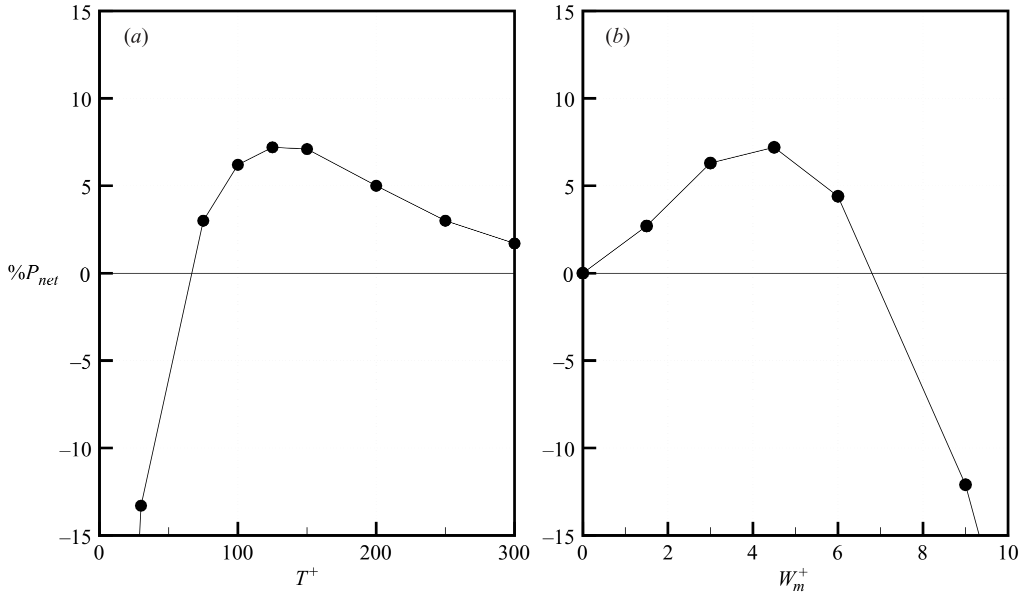

FIGURE 5. $\%P_{net}$ as (*a*) a function of the period of oscillation T^+, at $W_m^+ = 4.5$, and (*b*) as a function of maximum wall velocity W_m^+, at $T^+ = 125$.

of $\%P_{sav}$, but, as notable in figure 3, the drag reduction increase with W_m is linear or less than linear, while viscous losses increase quickly with W_m. Indeed, the laminar analysis by Quadrio & Ricco (2003) suggests a quadratic dependence on W_m, which is supported by the present data. The maximum saving is located around the optimum value of the period (i.e. $T^+ \approx 125$) and at small values of the maximum wall velocity, around $W_m^+ = 4.5$.

A better quantitative look at the same data can again be taken by means of sections of the three-dimensional space, at constant velocity or at constant period. Figure 5 (*a*) shows net percentage drag-reduction values as function of T^+ for $W_m^+ = 4.5$. The net balance is positive for $T^+ > 70$ and maximum for $T^+ = 125$. The maximum value of $\%P_{net}$ is 7.3, which can perhaps be regarded as an interesting high value. We recall that other passive drag-reduction techniques, for example riblets (Bechert *et al.* 1997), are considered interesting from a practical point of view, while providing comparable values of drag reduction. Figure 5(*b*) shows how $\%P_{net}$ varies with W_m^+ at $T^+ = 125$: we can appreciate that a positive balance occurs for $0 < W_m^+ < 7$.

4. Discussion

The present measurements should be put in the context of already existing data related to the oscillating-wall technique. In this section, we discuss the open issues mentioned in § 1, in view of the results reported so far.

4.1. *Maximum drag reduction and dependence of drag reduction on the oscillation parameters*

To start the discussion, we again note that all the numerical studies available in the literature (Jung *et al.* 1992; Baron & Quadrio 1996; Nikitin 2000; Quadrio & Sibilla 2000; J.-I. Choi *et al.* 2002) have found that the maximum drag-reduction is of the order of 40%. The present study is in agreement with this finding. On the other hand,

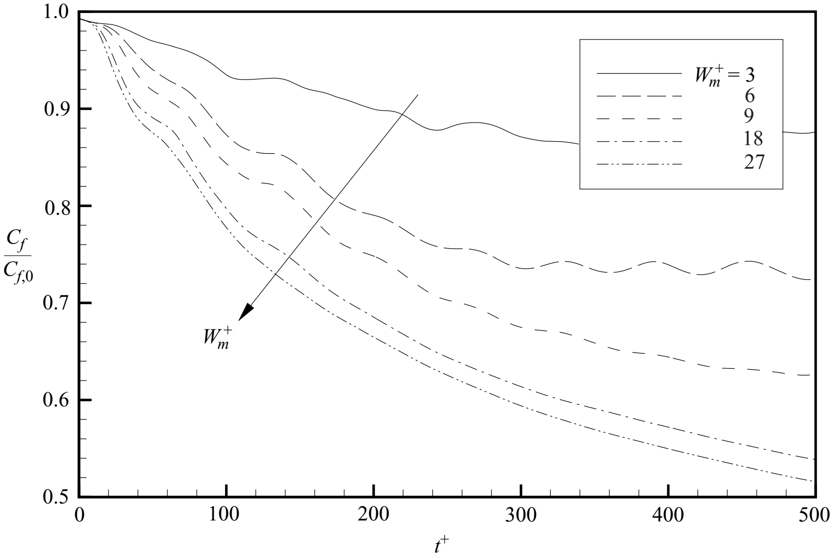

FIGURE 6. Transient behaviour of friction at $T^+ = 125$, for different values of W_m. The time history of the wall-averaged friction is ensemble-averaged over the two walls.

most of the experimental investigations conducted to date (Laadhari *et al.* 1994; Trujillo *et al.* 1997; Choi & Graham 1998) have reported substantially lower skin friction decrements, quantified at 35%, 27% and 25%, respectively. These differences are high, indeed larger than the reasonable uncertainty in measurements.

Experiments are typically carried out at values of the Reynolds number slightly higher than the numerical simulations. The question of whether the drag-reduction properties of the oscillating wall can be exploited in high-*Re* flows still requires a definite answer, but Choi & Graham (1998) have found that, for relatively small variations of the Reynolds number, the effects should be quite small. Hence, Reynolds-number effects cannot, by themselves, explain significantly different values of drag reduction.

A further significant difference between laboratory experiments and numerical simulations is that, in the latter, the moving wall has an indefinite extension, as implied by the periodic boundary conditions, while in an experiment only a finite section of the wall is oscillated. It follows that the initial temporal transient after the start-up of the oscillations must be discarded in numerical simulations, as we have done in the present work by following the procedure described in § 2.3. In experiments, on the other hand, the temporal transient does not bear particular significance (provided that data acquisition is not started at the same time the movement of the wall). However, the spatial transient must be properly accounted for when deciding the position of the measuring probe. Only Choi *et al.* (1998) have measured the local friction coefficient along the streamwise coordinate, starting from the leading edge of the oscillating plate. They noted that their oscillating section (3500 viscous lengths) could have been insufficiently long (it is said to be 'marginal' in their paper). Furthermore, they took most of the measurements 70 viscous lengths downstream of the trailing edge of the oscillating plate. Their measurements of local friction along the streamwise direction were taken at the sole oscillating condition of $W_m^+ = 7$ and $T^+ = 185$.

In the present study, we are limited to addressing the temporal transient. Figure 6 shows the decrease of friction versus time for various computational cases, measured from the very beginning of the wall oscillation. It is evident that, for a given T^+, the time required by friction to approach its asymptotic value significantly increases with W_m^+, as recently highlighted by Quadrio & Ricco (2003). A temporal transient can be converted into a spatial one by using Taylor's frozen-equilibrium hypothesis, and the concept of convection velocity. Kim & Hussain (1993) and, more recently, Quadrio & Luchini (2003) determined a convection velocity of $\approx 10 u_\tau$ for the wall-friction fluctuations. For $W_m^+ = 6$, a transient time of $t^+ = 300$–400 can thus be estimated from figure 6, which implies a transient region of 3000–4000 viscous lengths, in line with the aforementioned measurement of Choi *et al.* (1998) at $W_m^+ = 7$.

The important point is that, in analogy with the transient time interval of temporal simulations, the transient length in experiments is expected to increase with W_m. We can then estimate that the length at $W_m^+ = 18$ could be 2–3 times the length at $W_m^+ = 6$. Drag-reduction measurements at high values of W_m reported in Laadhari *et al.* (1994), Skandaji (1997), Trujillo *et al.* (1997), Choi *et al.* (1998, later discussed in Choi 2002) might then have been conducted not sufficiently downstream from the leading edge of the oscillating section of the plate. Indeed, in none of the published experiments did the location of testing along the streamwise coordinate vary, whereas both W_m and T changed substantially. The testing distance from the leading edge of the moving walls was 2650 viscous lengths for the measurements described in Choi (2002, where W_m^+ up to 16 were tested), 3200 for Laadhari *et al.* (1994) and Skandaji (1997) (W_m^+ up to 16), and 4200 for Trujillo *et al.* (1997) (W_m^+ up to 17).

Although the previous analysis suggests that the spatial transient might have caused biased measurements and, in turn, slightly lower amounts of drag reduction, it does not adequately explain why discrepancies as high as 20% on the amount of maximum drag reduction occur between numerical and experimental results. We conjecture that drag reductions as high as 40% were never measured in the laboratory because the parameters of the oscillations were never set within the optimal range, which, by observing figure 1, could be identified by $D_m^+ > 500$, $60 < T^+ < 140$ and $W_m^+ > 17$.

An additional discrepancy between numerical and experimental studies is that the latter indicate a monotonic increase of the amount of drag reduction with decreasing T at fixed D_m. On the other hand, moving towards low values of T^+ along one of the hyperbolae at fixed D_m^+ shown in figure 1, as experimentalists are forced to do, the amount of drag reduction should first increase and then decrease to zero. From our data, this is particularly evident in the region of $D_m^+ < 200$. We explain this discrepancy by observing that in none of the experiments were the periods so low as to exceed the optimum. One case in which perhaps the optimum T has been experimentally reached is reported by Trujillo *et al.* (1997), where drag-reduction starts to decrease after $T^+ \approx 80$ with $D_m^+ = 240$. However, the investigators were not allowed to make any definitive comment, given the small friction decrease compared with their uncertainty range. Choi & Graham (1998), in a cylindrical pipe flow with a very long oscillating section, have presented a maximum 25% drag reduction at $Re_\tau \approx 530$ and $Re_\tau \approx 800$. As already pointed out by Quadrio & Sibilla (2000), the lower drag-reduction values at high W_m are at least partially due to non-optimal values of oscillation periods. Similarly to the above-mentioned experimental investigations, drag reduction kept increasing asymptotically by decreasing the period of oscillation, for a fixed D_m, so that the existence of a plateau region at low T was proposed. A sole measured point suggested the existence of an optimal period at $T^+ \approx 120$, but again the uncertainty range comprised the two highest drag-reduction values, and no data were acquired at lower oscillation periods. The issue of the optimum T^+ for fixed D_m^+ will be further addressed in §4.3.

In concluding this section, we observe that the significant friction increase reported by Jung *et al.* (1992) at $T^+ = 500$ has not been confirmed by our data. The suggestion put forward by Nikitin (2000) that a small amount of drag reduction could still be observable at even larger values of T^+, namely $T^+ \geqslant 1250$, is not addressed in the present simulations, owing to computational costs.

4.2. *Net energy saving*

The present results demonstrate that a net power saving is attainable by means of spanwise wall oscillations. This confirms and extends the findings by Baron & Quadrio (1996) and Quadrio & Sibilla (2000). Although it was on the basis of preliminary under-resolved calculations, they were the first ones to address the problem of the global energy budget, by comparing the power saved through the reduction in streamwise wall-shear stress with the power spent on moving the wall. Baron & Quadrio (1996) showed that an overall benefit can be achieved for maximum wall velocities $W_m^+ < 9$ and a period of oscillation $T^+ = 100$, with a maximum of 9–10% at $W_m^+ = 4.5$. Quadrio & Sibilla (2000), for the turbulent pipe flow, reported that a net gain of about 5–7% can be attained if T^+ remains within the 100–150 range. They also remarked that the maximum wall velocity above which the global energy budget becomes negative is $W_m^+ \approx 7$. The present results compare well with these findings and hence definitely assess the possibility of a significant net energetic benefit.

4.3. *Scaling of drag reduction*

Data in figure 3, corresponding to various combinations of T^+ and D_m^+, indicate that W_m^+ is probably the most influential parameter affecting drag reduction: they present a similar trend and a reasonable collapse, as long as periods not too far from the optimum are considered. However, it is our opinion that figure 3 does not support the idea of drag reduction simply scaling with W_m^+ over the entire range $0 < T^+ < 750$.

The argument on the spatial transient discussed in § 4.1 could explain why some experimentalists (Trujillo *et al.* 1997; Choi *et al.* 1998; Choi & Graham 1998; Choi 2002) support the idea of drag reduction scaling with W_m. An apparent scaling with W_m might indeed emerge for measurements influenced by the spatial transient, where drag reduction does not show a significant dependence on T, as verified by Quadrio & Ricco (2003). For measurements not influenced by transient problems, namely at low W_m and hence with low drag reductions, it could be that experimentalists considered the data which showed the optimal period to be within the uncertainty range.

We therefore want to determine a scaling parameter for the amount of drag reduction which is a function of both W_m^+ and T^+ (and, implicitly, of D_m^+). The parameter should account for the effect of the transversal boundary layer created by the alternate movement of the wall and described by the laminar solution of the so-called Stokes second problem (Schlichting & Gersten 2000):

$$w^+\left(y^+, t^+\right) = W_m^+ \exp\left(-y^+\sqrt{\pi/T^+}\right) \sin\left(\frac{2\pi}{T^+}t^+ - y^+\sqrt{\frac{\pi}{T^+}}\right). \qquad (4.1)$$

The coincidence between the laminar Stokes solution and the turbulent space-averaged spanwise flow has been verified by Quadrio & Sibilla (2000) for the cylindrical geometry of pipe flow, and by J.-I. Choi *et al.* (2002) for the planar geometry of channel flow. Quadrio & Ricco (2003) have found that this also occurs during the first instants of the wall motion, if the transient Stokes solution for a wall set in oscillatory motion is considered.

J.-I. Choi *et al.* (2002), starting from the Stokes solution, (4.1), suggested that a scaling parameter can be constructed by combining a wall-normal length scale ℓ related to the distance at which the wall oscillation affects the turbulent structures, and a local spanwise acceleration of the Stokes layer. The critical length scale, representative of the penetration depth of the Stokes layer into the turbulent flow, is identified by the requirement that the maximum oscillating velocity at a distance $y^+ = \ell^+$ from the wall has a magnitude higher than a threshold velocity W_{th}^+, representing a typical value of the spanwise turbulent fluctuations. The penetration depth can then be expressed, thanks to (4.1), as:

$$\ell^+ = \sqrt{\frac{T^+}{\pi}\ln\left(\frac{W_m^+}{W_{th}^+}\right)}.$$

The maximum spanwise acceleration a_m^+ during the cycle at a given distance $\overline{y}^+$ from the wall can be easily derived by differentiating (4.1) with respect to t^+, and is expressed by:

$$a_m^+ = \frac{2\pi}{T^+} W_m^+ \exp(-\overline{y}^+\sqrt{\pi/T^+}).$$

J.-I. Choi *et al.* (2002) chose (somewhat arbitrarily) $W_{th}^+ = 0.5$, since this value is within the maximum r.m.s. value of spanwise turbulent fluctuations. They also selected a_m^+ at $\overline{y}^+ = 5$, since the flatness distribution of the streamwise velocity fluctuations presents a local peak at that distance from the wall. The two quantities ℓ^+ and a_m^+ can then be united to form a third group:

$$S^+ = \frac{a_m^+ \ell^+}{W_m^+} = 2\sqrt{\frac{\pi}{T^+}\ln\left(\frac{W_m^+}{W_{th}^+}\right)} \exp(-\overline{y}^+\sqrt{\pi/T^+}). \tag{4.2}$$

After including the effect of the Reynolds number, J.-I. Choi *et al.* (2002) found a reasonably good correlation between the quantity S^+ and available drag reduction data, expressed in the form $\%P_{sav} = aS^+ + bS^{+2}$, with a and b being suitable coefficients determined from a least-squares fit.

The function $S^+ = S^+(T^+, W_m^+)$ described by (4.2) is qualitatively similar to the drag-reduction plot shown in figure 1: it goes to zero when $T^+ = 0$ and $T^+ \to +\infty$ (compare with figure 2), and has a logarithmic behaviour when $W_m \to +\infty$ (compare with figure 3). It presents a maximum w.r.t. T^+ for fixed W_m^+ that can be located by setting $\partial S^+/\partial T^+|_{W_m^+} = 0$. From

$$\ln\left(\frac{W_m^+}{W_{th}^+}\right) \frac{\pi}{(T^+)^2} \exp(-\overline{y}^+\sqrt{\pi/T^+}) \left(\overline{y}^+ - \sqrt{\frac{T^+}{\pi}}\right) = 0,$$

it follows that the maximum of S^+ at fixed W_m^+ is located at $T_{opt,W}^+ = \pi\overline{y}^{+2}$. This corresponds to $T_{opt,W}^+ = 25\pi \approx 78.5$ with the choice of parameters by J.-I. Choi *et al.* (2002), i.e. not too far from the observed optimal period $T_{opt,W}^+ \approx 125$.

In the definition, (4.2), of the scaling factor S^+, two free constants are present. Based on physical arguments, we can select $\overline{y}^+$ to fit the experimental data, since this distance alone determines the optimum period. If $T_{opt,W}^+ = 125$, it follows that $\overline{y}^+ = 6.3$. A value of W_{th}^+ of the order of the turbulence fluctuations should then be around $W_{th}^+ = 1$, as follows from the physical significance of the friction velocity. A quantitative approach to select the value of the two constants involves determining the correlation coefficient between the measured drag-reduction data and the scaling

$\overline{y}^+$	5.0	5.5	6	6.1	6.2	6.3	6.4	6.5
W_{th}^+								
0.5	0.9777	0.9853	0.9846	0.9837	0.9825	0.9812	0.9797	0.9780
0.75	0.9789	0.9895	0.9923	0.9921	0.9916	0.9910	0.9902	0.9892
1.0	0.9773	0.9897	0.9947	0.9950	0.9951	0.9949	0.9946	0.9941
1.1	0.9761	0.9890	0.9948	0.9952	0.9955	0.9955	0.9954	0.9950
1.2	0.9749	0.9882	0.9945	0.9951	0.9955	0.9958	0.9957	0.9955
1.3	0.9734	0.9871	0.9940	0.9947	0.9952	0.9955	0.9956	0.9955
1.4	0.9719	0.9858	0.9931	0.9939	0.9945	0.9950	0.9952	0.9953

TABLE 3. Correlation coefficient between drag reduction data $\%P_{sav}$ from table 2 (with $T^+ \leqslant 150$) and the value of S^+ from (4.2), as a function of the values of the free constants $\overline{y}^+$ and W_{th}^+.

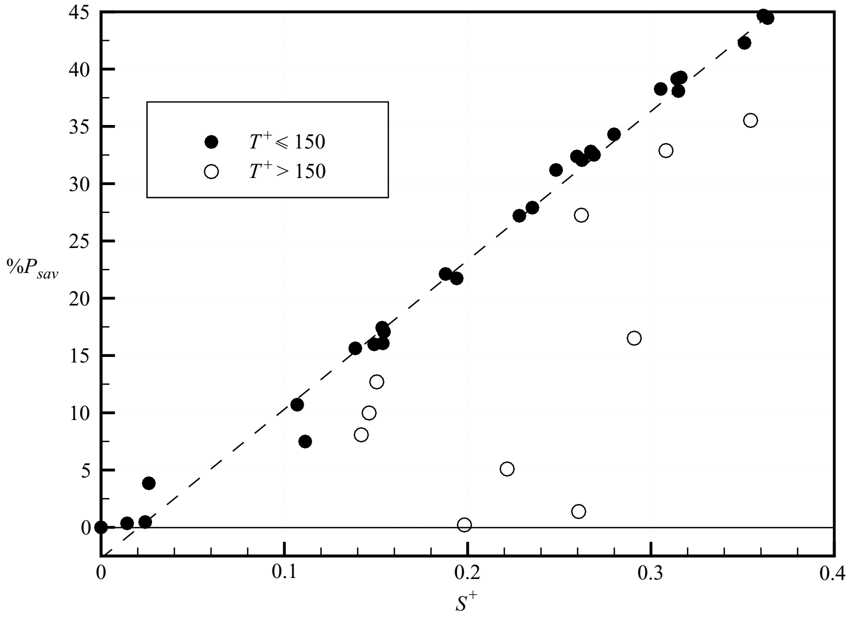

FIGURE 7. Drag-reduction data $\%P_{sav}$ from table 2 versus the parameter S^+, computed with $\overline{y}^+ = 6.3$ and $W_{th}^+ = 1.2$. The dashed line is the best fit to the filled circles, with equation $\%P_{sav} = 131S^+ - 2.7$.

factor S^+, by systematically changing $\overline{y}^+$ and W_{th}^+. Table 3 gives these coefficients (computed only for data with $T^+ \leqslant 150$, for the reason discussed below). It can be seen that the values providing the best linear regression of the data (i.e. $\overline{y}^+ = 6.3$ and $W_{th}^+ = 1.2$) are very close to the values dictated by physical considerations, even though not coincident with the values used by J.-I. Choi *et al.* (2002).

The present drag-reduction data are shown in figure 7 versus the parameter S^+, computed with $\overline{y}^+ = 6.3$ and $W_{th}^+ = 1.2$. The filled circles represent cases with $T^+ \leqslant 150$, and the correlation is high: almost all the data fall on a straight line, and the correlation is much stronger than the nonlinear (and scattered) one reported by J.-I. Choi *et al.* (2002). On the other hand, the empty circles, representing data with $T^+ > 150$, are much less correlated. Periods slightly higher than the optimum involve

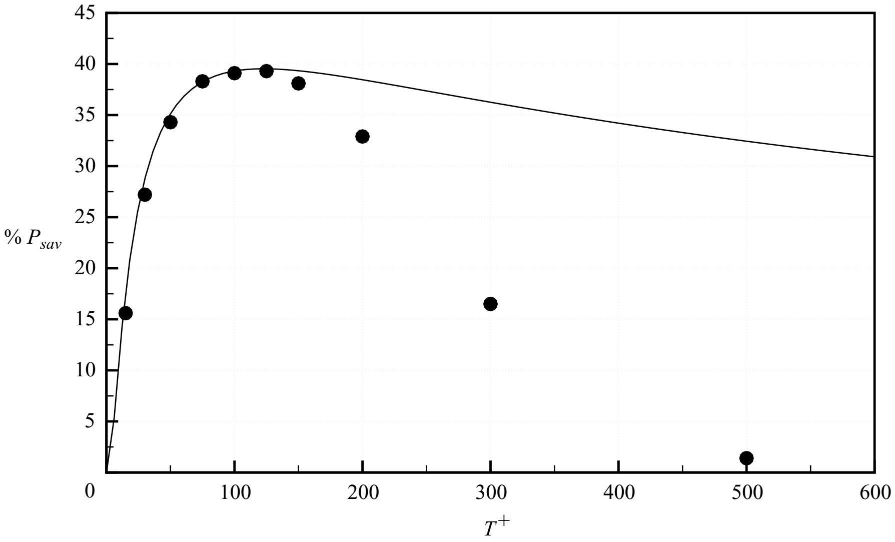

FIGURE 8. Comparison between $\% P_{sav}$ measured at different T^+ for $W_m^+ = 18$, and the function $131 S^+(T^+, 18) - 2.7$.

slight deviations from the straight line, whereas points at higher T^+ are at a greater distance. Data in these regions of the parameter space were not reported by J.-I. Choi *et al.* (2002).

The scaling parameter S^+ then appears not well suited for describing the drag modifications induced by a wall oscillating with very long period. Another way of looking at the same concept is reported in figure 8, where the drag reduction at different values of T^+ for a fixed $W_m^+ = 18$ is compared with the best fit to the function $S^+(T^+, 18)$. The agreement is very good for $T^+ \leqslant 150$. At higher periods, both functions tend to decrease, but the decrease rate of S^+ is much slower than that exhibited by the data.

We explain the behaviour of drag reduction values for $T^+ > 150$ by noting that the oscillation of the wall tends to become decoupled from the near-wall turbulence dynamics at high values of T^+. In their work on the integral space and time scales in wall turbulence, Quadrio & Luchini (2003) have shown that a typical pseudo-Lagrangian time scale can be computed for the near-wall turbulent structures, based on spatio-temporal correlation data. This characteristic time scale represents a typical survival time of the longest-lived and statistically significant turbulent structures. When computed for the longitudinal velocity fluctuations near the wall or for the longitudinal component of the wall friction, this time scale is about 60 viscous time units for a value of the Reynolds number very similar to the present one. The scaling parameter S^+ is then linearly related to the amount of drag reduction as long as the typical interaction time between the oscillating wall and the near-wall turbulent structures, namely $T^+/2$, is shorter than the typical longitudinal lifetime of the structures themselves. When T^+ is too long, the structures have enough time to develop their inner dynamics between successive sweeps of the transversal Stokes layer, and enough time is allowed for the near-wall turbulence to readapt to its natural equilibrium state, thus restoring the unperturbed value of friction drag.

The scaling factor S^+ also allows us to address the issue of the optimum period of oscillation $T^+_{opt,D}$ for fixed D_m^+. As previously discussed, it appears that none of the experimentalists support the existence of such a period, where as our results indicate

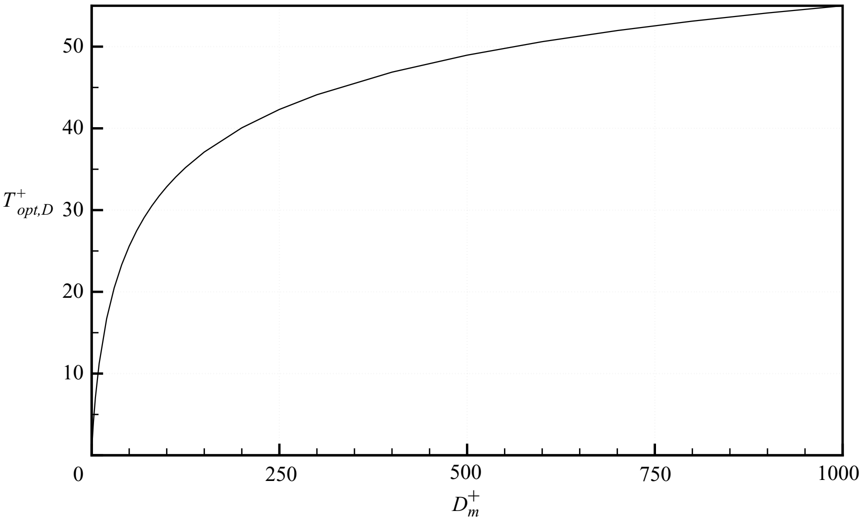

FIGURE 9. Optimum period of oscillation $T^+_{opt,D}$ as function of D^+_m.

that such a period is indeed a property of the oscillating-wall technique. Further, data in figure 1 suggest that $T^+_{opt,D}$ is lower than $T^+_{opt,W}$ for fixed W^+_m ($T^+_{opt,W} \approx 125$), although no definite conclusion can be drawn on whether and how $T^+_{opt,D}$ depends on D^+_m. As the scaling factor S^+ is very well linearly related to the amount of drag reduction (for $T^+ \leqslant 150$), we determine $T^+_{opt,D}$ by partial differentiation of the analytical expression (4.2) for S^+, after eliminating $W^+_m = \pi D^+_m / T^+$. Hence, by setting $\partial S^+ / \partial T^+|_{D^+_m} = 0$, we obtain the following implicit expression for $T^+_{opt,D}$:

$$\left(\overline{y}^+ \sqrt{\frac{\pi}{T^+_{opt,D}}} - 1\right) \ln\left(\frac{\pi D^+_m}{T^+_{opt,D} W^+_{th}}\right) = 2, \tag{4.3}$$

where $\overline{y}^+ = 6.3$ and $W^+_{th} = 1.2$ guarantee the best linear regression. Differently from $T^+_{opt,W}$, which does not depend on W^+_m, the period satisfying the above equation is related to D^+_m. Figure 9 shows that $T^+_{opt,D}$ increases monotonically with D^+_m, and that the rate of increment decreases with D^+_m. As expected, $T^+_{opt,D}$ is lower that $T^+_{opt,W}$. In figure 1, the dashed line represents the locus of points of $T^+_{opt,D}$, i.e. the solutions of (4.3) at various D^+_m. The predicted values of $T^+_{opt,D}$ agree with the (limited) measurement points along the hyperbolae of fixed displacement. We also notice that as the value of $T^+_{opt,D}$ tends to zero (and so does D^+_m), the corresponding value of $W^+_m \to W^+_{th} = 1.2$.

5. Conclusions

We have addressed some open issues related to the drag-reduction properties of a turbulent channel flow modified by wall oscillations, by carrying out a number of direct numerical simulations of the Navier–Stokes equations.

Amounts of drag reduction as high as 44.7% have been computed, so that previous numerical results have been confirmed. The drag reducing properties have been observed to depend on both the maximum wall velocity and the period of oscillation. We have provided an explanation for the discrepancies between numerical and experimental results, based on the analysis of the dependence of drag reduction on the parameters of the oscillation. Moreover, the possibility of achieving an overall positive energy balance has been assessed: a small but definite net energy saving can be attained, at least for the present value of the Reynolds number.

A parameter has been proposed, a function of both the maximum wall velocity and the period of the oscillation, which shows a linear correlation with the drag reduction data. The linear correlation holds as long as the half-period of the oscillation is shorter than a typical time scale of the flow, related to the survival time of the statistically significant near-wall turbulent structures. The same parameter also predicts that the period yielding the maximum drag reduction for fixed maximum wall velocity is constant, while the optimum period for fixed maximum wall displacement varies with the displacement itself.

This parameter could serve as a basis for further optimizations of the oscillating wall technique, aimed at maximizing the global energy budget by adjusting, for example, the temporal waveform of the oscillation. Before looking into possible applications of this technique, such optimizations must be investigated, together with the largely unknown dependence of its performance on the Reynolds number. The issue of the mechanical power spent in a real oscillating device must also be addressed. It may also be useful to recall that, in the case of confined flows (a pipeline, for example), energetic benefits comparable with those from the oscillating wall technique could be obtained with a small enlargement of the pipe diameter.

However, we emphasize that the fact that such a simple technique for turbulence control may yield a global energetic gain is a remarkable one. The present technique requires neither complicated feedback laws nor small-scale sensors or actuators. The success of the oscillating wall in reducing the turbulent friction with a positive energetic balance is a significant finding from a physical point of view, if we account for the strong tendency of turbulence to be attracted by its natural energy-consuming state.

The authors are indebted to Professor Paolo Luchini for illuminating discussions on the subject and for reading a preliminary version of the manuscript. Part of this work has been orally presented by P.R. at the 5th Euromech Fluid Mechanics Conference held in Toulouse, August 2003. Partial financial support from Italian Space Agency and Italian Ministry of University and Research is acknowledged.

REFERENCES

del Álamo, J. & Jiménez, J. 2003 Spectra of the very large anisotropic scales in turbulent channels. *Phys. Fluids* **15**, L41–L44.

Baron, A. & Quadrio, M. 1996 Turbulent drag reduction by spanwise wall oscillations. *Appl. Sci. Res.* **55**, 311–326.

Bechert, D., Bruse, M., Hage, W., van der Hoeven, J. & Hoppe, G. 1997 Experiments on drag-reducing surfaces and their optimization with an adjustable geometry. *J. Fluid Mech.* **338**, 59–87.

Berger, T. W., Kim, J., Lee, C. & Lim, J. 2000 Turbulent boundary layer control utilizing the Lorentz force. *Phys. Fluids* **12**, 631–649.

Choi, J.-I., Xu, C.-X. & Sung, H. J. 2002 Drag reduction by spanwise wall oscillation in wall-bounded turbulent flows. *AIAA J.* **40**, 842–850.

Choi, K.-S. 2002 Near-wall structure of turbulent boundary layer with spanwise-wall oscillation. *Phys. Fluids* **14**, 2530–2542.

Choi, K.-S., DeBisschop, J. & Clayton, B. 1998 Turbulent boundary-layer control by means of spanwise-wall oscillation. *AIAA J.* **36**, 1157–1162.

Choi, K.-S. & Graham, M. 1998 Drag reduction of turbulent pipe flows by circular-wall oscillation. *Phys. Fluids* **10**, 7–9.

Dean, R. 1978 Reynolds number dependence of skin friction and other bulk flow variables in two-dimensional rectangular duct flow. *Trans. ASME* I: *J. Fluids Engng* **100**, 215.

Dhanak, M. & Si, C. 1999 On reduction of turbulent wall friction through spanwise oscillations. *J. Fluid Mech.* **383**, 175–195.

Du, Y., Symeonidis, V. & Karniadakis, G. E. 2002 Drag reduction in wall-bounded turbulence via a transverse travelling wave. *J. Fluid Mech.* **457**, 1–34.

Jung, W., Mangiavacchi, N. & Akhavan, R. 1992 Suppression of turbulence in wall-bounded flows by high-frequency spanwise oscillations. *Phys. Fluids* A **4**, 1605–1607.

Karniadakis, G. & Choi, K.-S. 2003 Mechanisms on transverse motions in turbulent wall flows. *Annu. Rev. Fluid Mech.* **35**, 45–62.

Kim, J. & Hussain, F. 1993 Propagation velocity of perturbations in turbulent channel flow. *Phys. Fluids* A **5**, 695–706.

Kim, J., Moin, P. & Moser, R. 1987 Turbulence statistics in fully developed channel flow at low Reynolds number. *J. Fluid Mech.* **177**, 133–166.

Laadhari, F., Skandaji, L. & Morel, R. 1994 Turbulence reduction in a boundary layer by a local spanwise oscillating surface. *Phys. Fluids* **6**, 3218–3220.

Lele, S. 1992 Compact finite difference schemes with spectral-like resolution. *J. Comput. Phys.* **103**, 16–42.

Moser, R., Kim, J. & Mansour, N. 1999 Direct numerical simulation of turbulent channel flow up to $Re_\theta = 590$. *Phys. Fluids* **11**, 943–945.

Nikitin, N. V. 2000 On the mechanism of turbulence suppression by spanwise surface oscillations. *Fluid Dyn.* **35**, 185–190.

Orlandi, P. & Fatica, M. 1997 Direct simulations of turbulent flow in a pipe rotating about its axis. *J. Fluid Mech.* **343**, 43–72.

Quadrio, M. & Luchini, P. 2001 A 4th order accurate, parallel numerical method for the direct simulation of turbulence in Cartesian and cylindrical geometries. In *Proc. XV AIMETA Conf. on Theor. Appl. Mech.*

Quadrio, M. & Luchini, P. 2003 Integral time-space scales in turbulent wall flows. *Phys. Fluids* **15**, 2219–2227.

Quadrio, M. & Ricco, P. 2003 Initial response of a turbulent channel flow to spanwise oscillation of the walls. *J. Turbulence* **4**, 007.

Quadrio, M. & Sibilla, S. 2000 Numerical simulation of turbulent flow in a pipe oscillating around its axis. *J. Fluid Mech.* **424**, 217–241.

Schlichting, H. & Gersten, K. 2000 *Boundary-Layer Theory*. Springer.

Skandaji, L. 1997 Etude de la structure d'une couche limite turbulente soumise à des oscillations transversales de la paroi. PhD Thesis, Ecole Centrale de Lyon.

Trujillo, S., Bogard, D. & Ball, K. 1997 Turbulent boundary layer drag reduction using an oscillating wall. *AIAA Paper* 97-1870.